Thermal effects of substrate on Marangoni flow in droplet evaporation: Response surface and sensitivity analysis

Xue Chen [a,b], Xun Wang [b,1], Paul G. Chen [b], Qiusheng Liu [a,c,*]

[a] Key Laboratory of Microgravity, Institute of Mechanics, Chinese Academy of Sciences, Beijing 100190, China
[b] Aix Marseille Univ, CNRS, Centrale Marseille, M2P2, Marseille, France
[c] University of Chinese Academy of Sciences, Beijing 100049, China

ABSTRACT

In this paper, the evaporation of sessile droplets resting on a substrate with different thermal properties is numerically investigated. Computations are based on a transient axisymmetric numerical model. Special attention is paid to evaluate thermal effects of substrate on the structure of bulk fluid flow in the course of evaporation. Numerical results reveal that Marangoni convection induced by non-uniform distribution of temperature along the interface exhibits three distinctly different behaviours: inward flow, multicellular flow and outward flow, consequently resulting in different particle depositions. It is highlighted that three factors (i.e. relative thermal conductivity, relative substrate thickness and relative substrate temperature) strongly affect the flow pattern. In order to further investigate the coupling effects of different influential factors, a Kriging-based response surface method is introduced. We model the flow behaviour as a function of continuous influential factors using a limited number of computations corresponding to discrete values of the inputs. The sensitivities of the Marangoni flow are also analysed using Sobol' index to study the coupling mechanisms of influential factors. The proposed method can be used to forecast the flow patterns for any input parameter without additional sophisticated computer simulation, and allows to confidently estimate an unknown environmental parameter.

1. Introduction

The evaporation of a liquid drop resting on a solid substrate is not only of fundamental scientific interest but also of great importance in a wide variety of industrial and scientific applications, such as evaporative self-assembly technique (DNA mapping, MEMS cooling) [1,2], evaporation-induced particle deposition (thin film coating, ink-jet printing) [3,4] and the design of more efficient heat transfer devices [5]. Among the mechanisms involved, the behaviour of Marangoni flow induced by temperature gradient along the liquid-gas interface can significantly influence deposition patterns upon drying. For this reason, understanding the flow characteristics inside the drop plays a vital role in controlling the distribution of the particle deposition in evaporating droplet.

Extensive theoretical and experimental researches have been motivated in recent years [6–8]. Most of the previous works were based on diffusion-limited process, normally focusing on predicting the evaporation rate. Hu & Larson [9] suggested a simple approximation to summarise the total mass flux across the droplet surface and then in turn to solve the free-surface problem. Other investigations like Ruiz & Black [10] provided insight into revealing the mechanisms within the liquid drop. Similarly, the experimental work by Girard et al. [11] explained that the flow inside the drop was induced by the non-uniform temperature distribution along the interface. Although surface-tension-driven flow (i.e. Marangoni flow) and resultant bulk flow have been extensively studied, the influence of thermal effects of the substrate on Marangoni flow patterns is less well-understood. Further theoretical analysis has pointed out that the direction of Marangoni flow is determined by both the relative thermal conductivity [12] and the relative substrate thickness [13], ultimately alters the deposition patterns. However, these investigations were limited to the case of non-heated substrate; the impact of substrate temperature was not taken into account. Furthermore, the above-mentioned studies were based on a pseudo-transient process which implies that the

Nomenclature

r, z	cylindrical coordinates [m]
R	contact radius [m]
h_s	substrate thickness [m]
T	temperature [°C]
H	relative humidity
p	hydrodynamic pressure [N/m^2]
k	thermal conductivity [W/m K]
c_p	specific heat capacity [J/kg K]
D_0	diffusion coefficient [m^2/s]
K	mean curvature [m^{-1}]
c	molar concentration [kg/m^3]
u_Γ	normal velocity of the liquid-gas interface [m/s]
H_{vap}	latent heat of evaporation [J/kg]
j_m	local evaporation flux [kg/m^2 s]
J_m	overall evaporation flux [kg/s]
R_N	relative thermal resistance
CV_s	cross-validation value
S_{θ_i}	Sobol' index
f_{θ_i}	response surface for different contact angles

Greek symbols

θ	contact angle [°]

σ	surface tension [N/m]
σ_T	surface tension coefficient [N/m K]
ρ	density [kg/m^3]
μ	dynamical viscosity [Pa s]
α	thermal diffusivity [m^2/s]

Subscripts

0	initial or reference condition
∞	at the infinite in the gas region
l, s, g	liquid, solid, gas

Superscripts

*	dimensionless variable

Acronyms

LOO	Leave-One-Out
RE	Relative Error
RSM	Response Surface Method
SSA	Sobol Sensitivity Analysis

solution is a steady-state solution rather than a pure transient one. In this paper, we present numerical computations on the evaporation of sessile droplets resting on a heated substrate; we are particularly interested in evaluating thermal effects of the substrate on Marangoni flow in the course of evaporation, and determining typical bulk flow structures as a function of influential parameters related to the substrate. Indeed, based a transient, fully coupled three-phase (liquid-solid-gas) model, we clearly determined three distinct behaviours of Marangoni flow inside an evaporating droplet.

The efficient numerical technique is a more reliable tool for simulating the droplet evaporation process owing to its capability to consider the fully coupled mechanisms, like heat and mass transfer, thermal effects of substrate, evaporative cooling and thermocapillary convection [14,15]. In the present work, the effects of the substrate on Marangoni flow with respect to the influential parameters (thermal conductivity, thickness and substrate temperature) in a wide range are investigated. For this purpose, we need to simulate the evaporation process for all the possibilities of influential parameters. An alternative approach is to utilise response surface method (RSM). This approach aims to construct a continuous function of output by Kriging method [16,17], which allows to use the numerical results as a black-box with a limited number of inputs and outputs, and has proven to be a particularly effective tool for understanding fluid dynamics mechanisms and acoustic problems [18–22]. A leave-one-out (LOO) cross validation strategy [23] can be adopted to evaluate the reliability of the constructed response surface. Besides, the sensitivity analysis via Sobol' index [24,25] is able to quantify the relative importance of each input parameter in determining the response variability. By the Kriging-based response surface, the numerical results for any input model data can be rapidly forecast without further numerical computation. In terms of inverse problem, the Kriging-based response surface also helps to estimate the unknown input. It may happen in space experiments that some important input parameters, e.g. liquid concentration field in the vapour phase cannot be measured. In this case, the aforementioned unknown parameters can be estimated using the experimental results and the proposed response surface. The accuracy of parameter estimation strongly depends

on the sensitivity of input parameters according to Sobol' sensitivity analysis (SSA). To the best of our knowledge, investigating the coupling mechanisms of multi-parameter on Marangoni flow by RSM and SSA, has not been reported in the literature.

The present paper aims to understand the behaviour of Marangoni flow in evaporating droplets and thus may be helpful to predict and control the deposition patterns in drying droplets. It is organised as follows. A transient axisymmetric numerical model for a sessile droplet evaporating on a heated substrate is developed in Section 2. Section 3 introduces a novel method based on RSM and SSA to evaluate the thermal effects of substrate on the structure of bulk flow induced by thermocapillarity. Results of single influential factor and the coupling mechanisms of multiple factors are presented and discussed in Section 4. Finally, the conclusions resulting from this investigation are summarised in Section 5.

2. Mathematical model

We consider a sessile drop with an initial contact angle θ_0 and a contact radius R_0 resting on a heated substrate of thickness h_s, as shown in Fig. 1. It is assumed that an axisymmetric sessile droplet
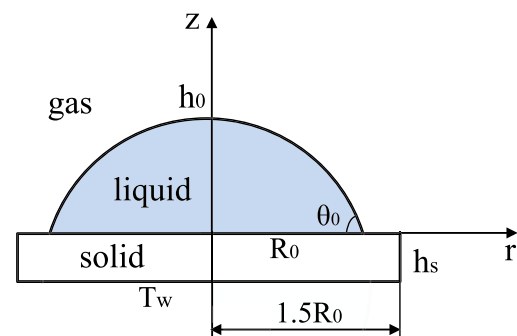

Fig. 1. A sessile drop resting on a heated substrate in a cylindrical coordinate system with radial coordinate r and axial coordinate z. The outer boundary of the computational domain is selected up to $50R_0$ of the surrounding air in order to eliminate the boundary effects and minimise the computational cost.

maintains a spherical-cap shape due to the effect of liquid-gas surface tension $\sigma = \sigma_0 - \sigma_T(T - T_0)$, in which σ_0 and σ_T are the surface tension at the reference temperature T_0 and its (negative) gradient with temperature, respectively. Moreover, the buoyancy effect may be neglected in microgravity, i.e. Marangoni effect dominates the whole process. The bottom of the substrate is maintained at a temperature T_w while the gas far from drop is at temperature T_∞.

It is further assumed that the drop forms a constant contact line, i.e. the base radius of the drop remains pinned at $R = R_0$. The assumption of constant-radius model is consist with the evaporation process observed in our experiments. In our ground and space experiments, we used a solid substrate and injected sufficient liquid volume to make sure that the contact line is well anchored to the substrate with it radii being at the edge of the substrate. Under such conditions, the evaporation process observed follows essentially the constant-radius mode during most of the drop's lifetime (90%). Therefore, it can reasonably be assumed that the contact radius R remains uncharged in our numerical simulations.

The physical problem is mathematically described by the continuity equation and incompressible Navier-Stokes equations in the liquid phase, the energy equations in all the domain regions (liquid-solid-gas), complemented by the diffusion equation for vapour in the gas phase:

In the liquid phase:

$$\nabla \cdot \mathbf{u}_l = 0, \tag{1}$$

$$\rho_l(\partial_\tau \mathbf{u}_l + \mathbf{u}_l \cdot \nabla \mathbf{u}_l) = \nabla \cdot \left[-p_l\mathbf{I} + \mu_l\left(\nabla \mathbf{u}_l + (\nabla \mathbf{u}_l)^T\right) \right], \tag{2}$$

$$\partial_\tau T_l + \mathbf{u}_l \cdot \nabla T_l = \alpha_l \nabla^2 T_l, \tag{3}$$

in which $\mathbf{u}_l, p_l, \mathbf{I}, \mu_l, T_l$ are the liquid velocity vector, hydrodynamic pressure, identity tensor, dynamical viscosity and temperature, respectively. Here, $\alpha_l = k_l/\rho_l c_{pl}$ is the thermal diffusivity, whereas ρ_l, c_{pl} and k_l refer to density, specific heat capacity and thermal conductivity for the liquid.

In the gas phase, vapour and heat transport in the atmosphere are solely by diffusion:

$$\partial_\tau c = D_0 \nabla^2 c, \tag{4}$$

$$\partial_\tau T_g = \alpha_g \nabla^2 T_g, \tag{5}$$

where c stands for the molar concentration of the liquid vapour and D_0 is the diffusion coefficient of vapour in air. For simplicity, we only consider the fluid flow in the liquid phase, hence the advection in the gas phase is neglected.

In the solid phase (substrate), the heat transfer is due to heat conduction:

$$\partial_\tau T_s = \alpha_s \nabla^2 T_s. \tag{6}$$

The boundary conditions are described hereafter. The bottom of the substrate is maintained at a temperature T_w, in the range of 20–50 °C. Temperature continuity is applied at all the interfaces. The no-slip boundary condition is used at the solid-liquid interface and the non-permeable wall at the solid-gas interface. The continuity of heat flux is applied at both solid-liquid and solid-gas interfaces. On the outer boundary of the computational domain, chosen typically several dozens of times larger than the radius of drop, the values of an ambient temperature T_∞ and vapour concentration c_∞ are prescribed. More specifically, the ambient concentration $c_\infty = Hp(T_\infty)/\overline{R}T_\infty$, here, $p(T_\infty)$ is the pressure at ambient temperature T_∞ and $\overline{R} = 8.31451$ J/(mol K) is the universal gas constant.

At the liquid-gas interface, the condition of stress balance gives

$$(\mathbf{n} \cdot \mathbf{T}_l) \cdot \mathbf{n} = -(2\sigma K + p_\infty), \tag{7}$$

$$(\mathbf{n} \cdot \mathbf{T}_l) \cdot \tau = \sigma_T \nabla_\Gamma T, \tag{8}$$

in which $\mathbf{n}$ and τ are the unit normal and tangential vector to the liquid-gas interface (denoted by Γ), $\mathbf{T}_l$ $(= -p_l\mathbf{I} + \mu_l(\nabla \mathbf{u}_l + (\nabla \mathbf{u}_l)^T))$ stands for the full stress tensor of fluid, K is the mean curvature of the liquid-gas interface, and ∇_Γ denotes the gradient tangent to the interface. It is worth noting that the right-hand side of Eq. (7) represents the pressure inside a droplet at equilibrium while that of Eq. (8) describes the driving force of bulk flow, i.e. the thermocapillarity. A characteristic velocity can also be inferred from the balance between viscous force $\mu_l \nabla_\Gamma U$ and thermocapillarity $\sigma_T \nabla_\Gamma T$, which results in a characteristic velocity scale $U \sim \sigma_T \Delta T / \mu_l$.

For the concentration of vapour c_{sat} at drop surface, it assumes to be ideal gas and saturated according to the Clausius-Clapeyron equation, defined by

$$c_{sat}(T) = \frac{p_{sat}(T)}{\overline{R}T}, \tag{9}$$

$$\ln\left(\frac{p_{sat}(T)}{p_{ref}(T)}\right) = -\frac{H_{vap}}{\overline{R}}\left(\frac{1}{T} - \frac{1}{T_{ref}}\right), \tag{10}$$

where $p_{sat}(T)$ and $p_{ref}(T)$ are the pressure of saturated vapour at temperature T and T_{ref}, respectively.

The heat flux across the interface experiences discontinuity due to the latent heat of vaporisation H_{vap}:

$$k_g \nabla T_g \cdot \mathbf{n} - k_l \nabla T_l \cdot \mathbf{n} = j_m H_{vap}, \tag{11}$$

where j_m is the local evaporation flux, which can be calculated by Fick's law:

$$j_m = -D_0 \nabla c \cdot \mathbf{n}. \tag{12}$$

The condition of mass conservation across the interface leads to:

$$\rho_l(\mathbf{u}_l \cdot \mathbf{n} - u_\Gamma) = j_m, \tag{13}$$

where u_Γ is the normal velocity of the interface. We assume that the droplet remains a spherical-cap shape during the evaporation and that the contact line is pinned at $R = R_0$ (but the instantaneous contact angle θ decreases with time). Given the total mass evaporation flux $J_m = \int_\Gamma j_m d\Gamma$, the normal velocity can be geometrically determined:

$$u_\Gamma = -\frac{J_m}{\pi \rho_l R_0^2}\left(\sqrt{1 - \left(\frac{r\sin\theta}{R_0}\right)^2} - \cos\theta\right)\frac{1 + \cos\theta}{1 - \cos\theta}. \tag{14}$$

Since we are seeking a transient solution, the initial conditions also need to be prescribed. At $t = 0$, the drop is a spherical cap with height h_0 and base radius R_0 (initial contact angle θ_0 can be deduced by $\theta_0 = 2\tan^{-1}(h_0/R_0)$); the bulk flow inside the drop is at rest (i.e. $\mathbf{u} = 0$). The initial pressure within the drop is set to the ambient pressure augmented by the Laplace pressure ($\Delta p = 2\sigma_0/R_s$ with $R_s = (h_0^2 + R_0^2)/(2h_0)$). The initial temperature in the whole domain is set to an ambient temperature $T_\infty = 20$ °C. The drop evaporates into a non-saturated surrounding air with relative humidity $H = 50\%$ and the initial concentration in the vapour equals to $c_\infty = Hc_{sat}(T_\infty)$.

3. Response surface, sensitivity analysis and inverse problem

The purpose of the present work is to investigate how the thermal properties of a heated substrate affect the direction of Marangoni flow inside an evaporating drop. For a given input parameter, the droplet evaporation process can be numerically simulated, but the results cannot be realised for all the possible situations due to

the restricted computational resources. Therefore, the response surface is constructed using the Kriging method, as a function of concerned input parameters, via a limited number of simulations. With the Kriging-based response surface, the proposed results of the Marangoni flow pattern can be easily predicted. The reliability of the constructed response surface is evaluated via a LOO cross validation criterion. After that, in order to investigate the correlation of multiple parameter, the Sobol' sensitivity analysis method is introduced. Finally, an inverse problem is considered: in the case that one of the input parameters is ill-observed, it can be estimated via the Kriging-based response surfaces.

3.1. Response surface method

RSM is a useful tool to model the behaviour of a physical phenomenon with respect to the influential parameters variation, starting from a certain number of numerical experiments. Let Ω denote the considered input parameter space and $X(\omega)$ denote the quantity of interest (QoI), given n measurements $X(\omega_s)$ ($s = 1, \ldots, n$) at measured locations ω_s, the estimate of the QoI at an unmeasured location ω is a weighted linear combination:

$$\widehat{X}(\omega) = \sum_{s=1}^{n} \lambda_s(\omega)X(\omega_s), \tag{15}$$

in which $\lambda_s(\omega)$ is the Kriging weight depending on the concerned unmeasured location, more exactly the distance between the unmeasured sample location ω and the s-th sample location ω_s. The QoI $X(\omega)$ is decomposed into

$$X(\omega) = \beta(\omega) + \xi(\omega). \tag{16}$$

Here, the residual component $\xi(\omega)$ can be treated as a stationary random process with 0-mean and covariance $\mathrm{Cov}(\xi(\omega), \xi(\omega + \gamma)) = C(\gamma)$, where $C(\gamma)$ is called the covariance function, and $\beta(\omega)$ is a trend component. In this work, the spline covariance function is used to build the response surface, i.e.,

$$C(\gamma) = \begin{cases} 1 - 6(\gamma \varepsilon)^2 + 6(\gamma \varepsilon)^3, & \gamma < 1/2\varepsilon \\ 2(1 - \gamma \varepsilon)^3, & 1/2\varepsilon \leqslant \gamma < 1/\varepsilon, \\ 0, & \gamma \geqslant 1/\varepsilon \end{cases} \tag{17}$$

in which ε can be obtained via maximum likelihood estimation or empirical tuning.

The Kriging method minimises the variance of the estimator $\mathrm{Var}(\widehat{X}(\omega) - X(\omega))$ under the unbiasedness constraint $\mathbb{E}[\widehat{X}(\omega) - X(\omega)] = 0$, from which Kriging weights $\lambda_s(\omega)$ are obtained. It is remarkable that the Kriging estimate is a best linear unbiased predictor (BLUP). Actually, variant Kriging methods exist in the literature, among which Ordinary Kriging is used in this paper. This approach assumes that the trend component is constant but unknown, denoted as $\beta(\omega) = \delta_0$. The unbiasedness constraint implies that the sum of Kriging weights is equal to 1. Finally, minimising the error variance and adding a Lagrange parameter to fulfil the unbiasedness condition result in the Ordinary Kriging system:

$$\begin{cases} \sum_{j=1}^{n} \lambda_j(\omega)C(\omega_i - \omega_j) + \delta_0 = C(\omega_i - \omega) & i = 1, \ldots, n \\ \sum_{j=1}^{n} \lambda_j(\omega) = 1 \end{cases} \tag{18}$$

A response surface can be built with any number of samples, however, its reliability has to be assessed. Then, a LOO cross-validation strategy [23] is considered, which quantifies the relative variation of the constructed surface after removing one sample. The cross-validation value is expressed here as a global relative L_2 error:

$$CV_s = \frac{\sqrt{\int_{\Omega} \left(\widehat{X} - \widehat{X}^{-s}\right)^2 \mathrm{d}\omega}}{\sqrt{\int_{\Omega} \widehat{X}^2 \mathrm{d}\omega}}, \tag{19}$$

where $\widehat{X}^{-s}$ is the Kriging response surface built without the s-th sample. A threshold ε on the maximum cross-validation value is imposed to assess the convergence, i.e. $\max_s CV_s < \varepsilon$.

3.2. Sobol' sensitivity analysis

Sensitivity analysis is adopted to quantify the contribution of each input parameter to the response variability, as well as to assess the coupling effects related to the multiple parameters of the response surface. The sensitivity of the model with respect to the input parameters is quantified via Sobol' variance-based sensitivity indices [24], which are obtained from quasi Monte Carlo samples (Sobol sequences) [25]. The mean and variance estimates are obtained by

$$\overline{X} = \frac{1}{q_{MC}} \sum_{i=1}^{q_{MC}} \widehat{X}_i \tag{20}$$

and

$$\sigma^2(X) = \frac{1}{q_{MC}} \sum_{i=1}^{q_{MC}} (\widehat{X}_i - \overline{X})^2, \tag{21}$$

where q_{MC} is the number of quasi Monte Carlo samples obtained from the Kriging meta-model of $X(\Omega)$.

In order to compute the first-order sensitivity indices, two independent quasi Monte Carlo sample sets of Ω are generated, denoted as Ω_1 and Ω_2. Each of the sample set is a $q_{MC} \times D$ matrix and D is the number of input variables. The Sobol indices $S_j = \sigma_j^2 / \sigma^2$ for j-th variable is derived from the estimate of the variance and the partial variance σ_j^2:

$$\sigma_j^2 = \frac{1}{q_{MC}} \sum_{i=1}^{q_{MC}} \widehat{X}_i(\Omega_2)(\widehat{X}_i(\Omega_1^j) - \widehat{X}_i(\Omega_1)), \tag{22}$$

where Ω_1^j is the first samples set Ω_1 where the j-th column has been replaced by the corresponding column of the second sample set Ω_2.

3.3. Inverse problem

In this article, not only simulation and prediction referring to a forward problem is considered, but also the inverse problem, which consists in finding the optimal values for the input model parameters, is investigated. In the real experiments, some of the input parameters cannot be accurately measured, we can use the Kriging-based response surface to estimate the unknown input. Let ϕ be an unknown parameter and Φ be the set of other input parameters. The former can be estimated via the observed results θ and other input parameters:

$$\hat{\phi} = \arg\min_{\phi} |\theta_i - f_{\theta_i}(\phi, \Phi)|, \ i = 1, 2. \tag{23}$$

It is remarkable that both response surfaces can be used to estimate an unknown parameter. However, the one with higher reliability, which is quantified by the LOO criterion, is preferable, since the corresponding response surface has less local fluctuations which lead to a more robust estimation. Furthermore, the estimation accuracy of each parameter also depends on the sensitivity of the proposed response surface with respect to the corresponding

parameter, which is reflected by Sobol' index. In general, a parameter with higher sensitivity can be more accurately estimated, and vice versa.

4. Results and discussion

Numerical simulations of transient Marangoni flow together with heat and mass transfer have been performed using COMSOL Multiphysics. Numerical procedure and model validation can be found in [26]. In short, a grid sensitivity analysis has been first undertaken and grids consisting of 18,160 elements were selected to control the relative error within 1%. The computational domain is selected up to $50R_0$ of the surrounding air in order to eliminate the boundary effects and minimise the computational cost. As a further validation of the implemented numerical model, we first compare our numerical results with a previous work and explain three typical patterns of Marangoni flow inside an evaporating droplet. Then, thermal effects of substrate on the direction of Marangoni flow are investigated. In particularly, their coupling mechanisms are taken into consideration, using response surface method and Sobol' sensitivity analysis. Finally, the inverse problem is discussed for the ill-known influential parameter.

4.1. Marangoni flow pattern

We compare our numerical results with an asymptotic analysis reported in the literature [13], where a quantitative criterion to determine the direction of the induced Marangoni flow is described. The curve of the critical function $R_N = \alpha(\theta)$ is plotted in Fig. 2 together with the symbols obtained from our computations. Here, $R_N = h_s k_l / R_0 k_s$ is a non-dimensional parameter: the product of relative substrate thickness h_s/R_0 and relative thermal conductivity of liquid and substrate k_l/k_s. The analysis of Xu et al. [13] for a non-heated substrate indicates that for the values

of R_N above the curve, i.e. $R_N > \alpha(\theta)$, the resultant Marangoni flow is directed radially outward along the liquid-gas interface. On the contrary, if $R_N < \alpha(\theta)$, the temperature decreases with distance from the contact line to the apex, the direction of the flow is reversed. The presented numerical model for a sessile droplet evaporating on a heated substrate reproduces these features with respect to the direction of bulk flow. It is found that droplets evaporating on a heated substrate with poor thermal conductivity undergo a three-stage lifetime: inward flow (open symbol), multicellular flow (semi-filled symbol) and outward flow (filled symbol). It is worth noting that our numerical model is valid in a wider range of R_N whereas the analytical prediction is limited to small values of R_N, i.e. $R_N < 0.3$.

To better understand the physical phenomenon related to a poor thermal conductivity of the substrate, it is useful to first identify the structure of flow field within the drop; the velocity and temperature field are illustrated in Fig. 3. It can be seen that bulk flow exhibits different behaviours in the course of evaporation, which can be distinguished as: (a) Inward flow pattern: at the beginning the induced Marangoni flow is directed radially inward along the liquid-gas interface. Recall that the apex of the droplet is expected to be coolest due to a longer conduction distance from the substrate. As such, a positive tangential temperature gradient is generated from the droplet apex to the triple line, then Marangoni stress drives the hot water (near the triple line) to the cold region (at the top) resulting in an anticlockwise circulation; (b) Multicellular flow pattern: when the contact angle diminishes continuously during droplet evaporation and reaches a critical value θ_1, the surface temperature is no longer monotonic, consequently multiple clockwise and anticlockwise convective cells appear. The appearance of multicellular flow pattern refers to the breakup of the flow inside the droplet and corresponds to a nonmonotonic surface temperature function of r with maximal or minimal extremum along the interface due to convective instability; and (c) Out-
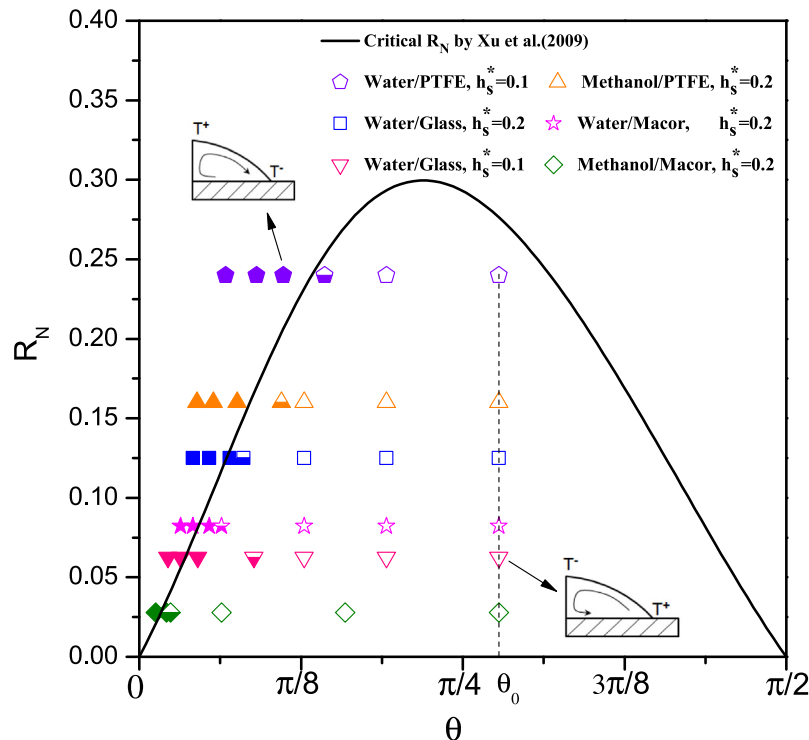

Fig. 2. The direction of Marangoni flow in evaporating droplets on non-heated substrates. The solid line is the asymptotic solution $R_N = \alpha(\theta)$ [13], where $\alpha(\theta) = [\sin(2\theta) - 4(1/2 - \theta/\pi) \tan(\theta/2)]/(4(1/2 - \theta/\pi) + 2\sin^2\theta)$ is a function of the contact angle. Computations are conducted for an initial contact angle $\theta_0 = 50°$ and instantaneous contact angle θ decreased with time. Regions above and below the line correspond to flow directions sketched in the figure; open symbol represents the inward flow, filled symbol stands for the outward flow and semi-filled symbol means the multicellular flow.
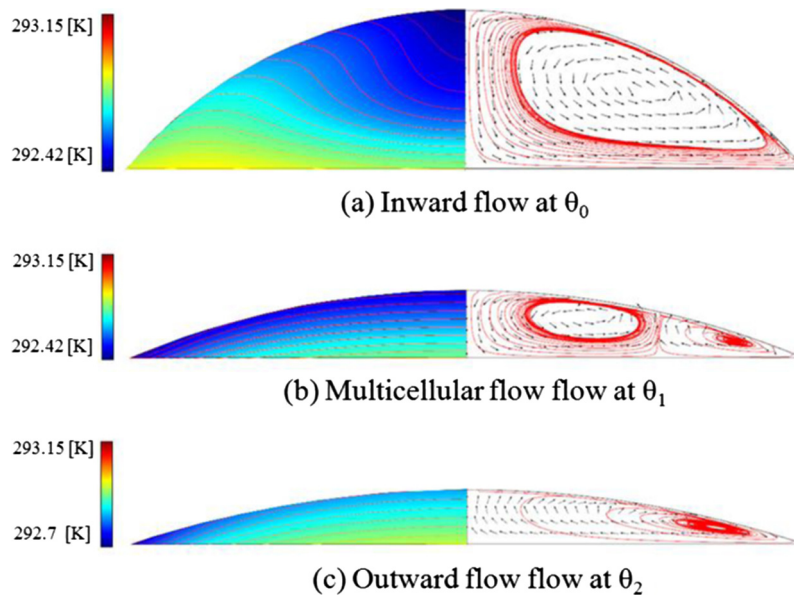
Fig. 3. Temperature field (left side) and bulk flow pattern (right side) within a water droplet evaporating on a PTFE substrate. Initial conditions: $\theta_0 = 50°, R_0 = 1$ mm, $h_s = 0.1$ mm, $T_\infty = T_w = 20$ °C, $H = 50\%$, and $p_\infty = 1$ atm. The streamlines are shown at different behaviours of Marangoni flow (denoted by three characteristic contact angles: θ_0, θ_1 and θ_2).

ward flow pattern: the temperature distribution is inverted with respect to outward flow. If the contact angle decreases below a threshold of θ_2, the energy is not readily supplied to the contact line region where the local heat flux is the largest. In this situation the heat conduction through the drop is dominant and the drop is warmest at the centre, thereby leading to an outward flow behaviour.

4.2. Thermal effects of substrate on Marangoni flow: single influential factor

In this section, the influence of thermal effects of substrate on the direction of Marangoni flow is numerically investigated. We highlight that during evaporation three influential factors determine the flow patterns inside the drop: relative thermal conductivity, relative thickness and relative substrate temperature. Each factor contributes to forming different structures of flow field and in turn controlling the particle deposition patterns.

4.2.1. Effect of relative thermal conductivity

The water drop evaporation with same initial conditions and various substrates is numerically studied. We choose six kinds of substrates, namely PTFE, glass, POM, PDMS, Macor and Al, for their widely differing thermal conductivities. Relevant physical properties of the liquids and substrates are listed in Table 1. It has been found that the thermal conductivities of the liquid and substrate strongly affect the structure of flow field [27]. In order to better characterise the influence due to thermal conductivities, we introduce a dimensionless number $k_r^* = k_l/k_s$ in the following discussion.

In Fig. 4, two characteristic contact angles as a function of the relative thermal conductivity k_r^* for a water droplet in the course of its evaporation are plotted. These two contact angles mark a transition of bulk flow pattern as a result of matching the heat transfer from the substrate and heat flux losing through the liquid-gas surface, associated with evaporative cooling effect. For a relative higher k_r^*, say $k_r^* > 0.5$, the bulk fluid flow clearly undergoes three different radial patterns as illustrated in Fig. 3: the transition from an inward flow to an outward pattern corresponds to the change of sign of the tangential component of the temperature gradient at the interface, passing through a multicellular flow pattern. In a manner similar to that observed in the coffee-ring problem [28], the particles ultimately assemble to the region near triple-line. In contrast, if k_r^* is extremely small ($k_r^* \rightarrow 0$), for instance, a water drop deposited on an Al substrate, then the energy provided from the substrate is enough for evaporation process, which results in an inward flow until the end of the evaporation. This can be explained by the fact that the area close to the triple-line is the warmest due to adjacent perfectly conducting substrate and the apex of the drop is colder, partially due to the long distance conduction. A similar behaviour was reported previously in [12] that Marangoni flow ultimately forces the particles toward to the centre and there will be no possibility for a multicellular flow arises.

Table 1
Physical properties of liquids and substrates used at temperature $T_\infty = 20$ °C and pressure $p_\infty = 1$ atm.

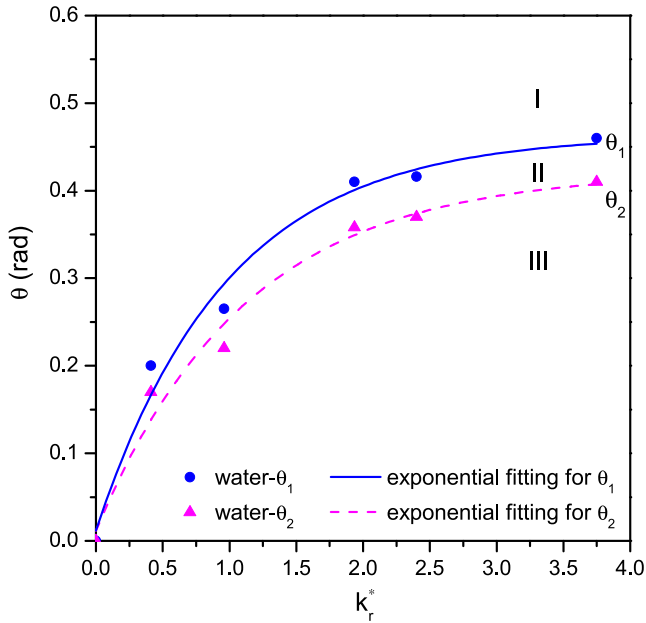| Parameter	ρ (kg/m^3)	μ (Pa s)	k (W/m K)	c_p (J/kg K)	H_{vap} (kJ/kg)	σ (N/m)	k_r^*
Water	997	0.89×10^{-3}	0.6	4070	2440	71.97×10^{-3}	
Air	1.178	1.79×10^{-5}	0.025	1006			
PTFE	2200		0.25	1010			2.4
Glass	2200		0.625	730			0.96
POM	1420		0.31	1500			1.935
PDMS	970		0.16	1460			3.75
Macor	2520		1.46	790			0.41
Aluminium	2700		240	900			0.0025

Fig. 4. Bulk flow pattern as a function of relative thermal conductivity $k_r^* = k_l/k_s$ for a water droplet evaporating on a substrate with bottom temperature $T_w = 20\,^\circ C$ and relative height $h_s^* = h_s/R_0 = 0.2$. Three typical flow structures are identified: region I (above the curve of θ_1) is an inward flow, region II (between the curves of θ_1 and θ_2) is a multicellular flow and region III (below the curve of θ_2) is an outward flow.

Fig. 5. Flow patterns inside evaporating drops with respect to relative thickness h_s^*. Here, $T_w = 20\,^\circ C$ and $k_r^* = 2.4$. Region I (above θ_1) is inward flow, region II (between θ_1 and θ_2) stands for multicellular flow and region III (below θ_2) represents outward flow.

4.2.2. Effect of relative thickness

We also study the dependence of Marangoni flow on the substrate thickness since it has similar role as the thermal conductivity [29]. Here, we define $h_s^* = h_s/R_0$ as relative thickness, representing the ratio of the substrate thickness to the contact radius of the droplet. Fig. 5 shows that the different regimes of convective Marangoni flow shift when the contact angle diminishes with respect to relative thickness. It displays that for a very thin substrate ($h_s^* \to 0$), the flow circulation is always radially inward due to a positive temperature gradient from apex to the triple-line. In this case heat transfer from the substrate dominates the whole process, hence surface temperature distribution remains monotonic corresponding to the inward flow of region I. Otherwise, the total amount of energy from the substrate is not enough to support evaporation and associated evaporative cooling effect, then convective multicellular flow occurs in region II and ultimately reverses the flow direction in region III.

4.2.3. Effect of relative substrate temperature

In terms of heated substrate, the evaporation rate is expected to be accelerated by higher temperature of substrate and consequently leads to enhance thermocapillary flow together with the appearance of multicelllular flow pattern. The objective here is to depict Marangoni flow transition with multiple relative substrate temperature $T_w^* = (T_s - T_\infty)/T_\infty$, that is, the relative difference between the substrate and ambient environment, ranging from 0 to 2. It can be concluded from the $T_w^* - \theta$ plane in Fig. 6 that at varied substrate temperature the convective multicellular flow occurs at the same contact angle θ_1, different from the other influential factors of k_r^* or h_s^*. The plotted curves also make it clear that the convective Marangoni flow lasts longer as the temperature becomes higher. This result is helpful for the prediction of particle deposition: multicellular flow pattern always appear at a certain height of droplet with respect to a wide range of substrate temperature during evaporation. If the deposition needs to be performed
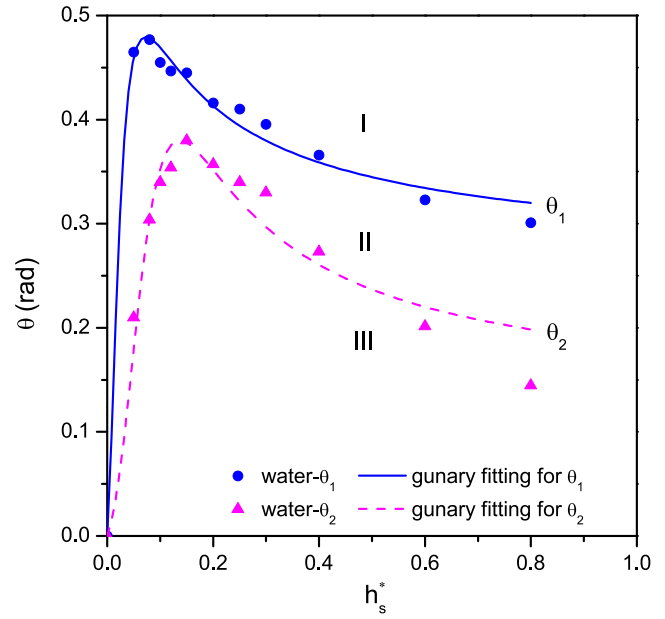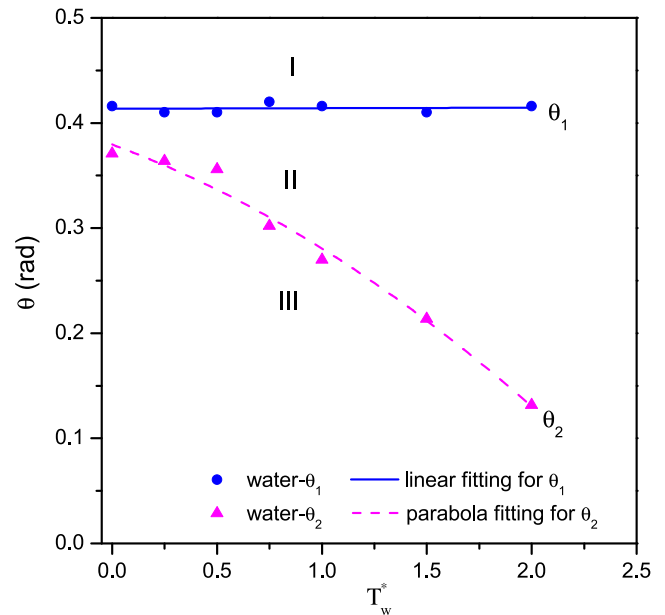

Fig. 6. Flow patterns inside evaporating drops corresponding to relative substrate temperature with $k_r^* = 2.4$ and $h_s^* = 0.2$. Region I above θ_1 is inward flow, region II between θ_1 and θ_2 stands for multicellular flow, and region III below θ_2 represents outward flow.

in a more regular pattern, then the substrate temperature must be decreased.

4.3. Coupling mechanisms of the substrate on Marangoni flow: multiple factors

In what follows, we attempt to emphasis the coupling mechanisms of multiple influential factors (k_r^*, h_s^* and T_w^*) by using

response surface method and Sobol' sensitivity analysis. It is the first study of its kind in solving the coupling effects on Marangoni flow by using the novel method RSM and SSA. In this section, we pay attention to three highlighted issues. The first one is to predict the multicellular flow pattern at any possible model input in a given range using RSM. Secondly, we analyse the coupling mechanisms via SSA. Finally, the inverse problem in terms of estimating unknown input parameter is discussed.

4.3.1. Predict the multicellular flow pattern using RSM

Since the internal flow pattern subjects to a wide range of influential parameters, it is impossible to compute all the possibilities due to the high computational cost. To globally evaluate the correlation between different influential factors, Kriging-based response surfaces are built with a limited number of various (k_r^*, h_s^*) and (R_N, T_w^*), consequently the Marangoni flow patterns for any input value in a given range could be rapidly forecast.

At first, the correlation of relative thermal conductivity and relative thickness is studied. A regular grid with 20 samples in (k_r^*, h_s^*) is used, which is shown by the crosses in Fig. 7. Generally speaking, the required number of samples of the grid depends on the dimension of the input parameters, the physical range of each input parameter and the complexity of the response. In this case, the 20-sample grid is proven to be reasonable such that the Kriging response surface converges; further tests with additional samples do not significantly increase the response surface reliability. Then, the response surfaces for the flow patterns reflected by the characteristic angles θ_1 and θ_2 are constructed using the Kriging method, as is shown in Fig. 8. The two surfaces represent the three behaviours of Marangoni flow: inward flow (I), multicellular flow (II) and outward flow (III), which are separated by the response surfaces f_{θ_1} and f_{θ_2}. The colormaps (b) and (c) are the projections of f_{θ_1} and f_{θ_2} in the (k_r^*, h_s^*) plane, respectively. To further assess the validity of the Kriging-based response surface, the LOO cross-validation is computed: the maximum cross-validation are respectively $\max_s CV_s(\theta_1) = 1.44\%$ and $\max_s CV_s(\theta_2) = 3.98\%$, which means that the second response surface is less robust due to more irregular observations from the sample points.

Then, the Marangoni flow pattern could be simply forecast via the constructed response surface without further numerical simulation, within the range of $k_r^* \in [0, 3.75], h_s^* \in [0.1, 0.4]$. Here, we

consider six samples, which are labelled by the circles in Fig. 7. For each case, the corresponding critical angles θ_1 and θ_2 are computed via the numerical simulations and compared with the output of the response surfaces. The forecast value and the corresponding relative error (RE) for the six points obtained from the surfaces f_{θ_1} and f_{θ_2} are shown in Table 2. By given the used liquid and substrate ($k_r^* = 3.16$) and geometrical parameters like initial contact radius and substrate thickness ($h_s^* = 0.2$), we can easily forecast the convective multicellular flow occurs at $\theta_1 = 0.4529$ and disappears at $\theta_2 = 0.3788$ from the response surfaces. The observed value of numerical simulation shows that the multicellular flow is at 0.454 and 0.384 for different contact angle θ_i, which demonstrates a good agreement. It is clear that θ_1 is accurately forecast by the Kriging-based response surface at all the six points with a mean RE being 1.56%. By contrast, the forecast of θ_2 is less accurate whose mean RE is around 4%, but in general the error is acceptable. Actually, the higher error of θ_2 forecast can be explained by the lower reliability of the response surface f_{θ_2}, which can be observed from Fig. 8 and justified by the LOO cross-validation values.

We now study the correlation between relative thermal resistance and relative substrate temperature (R_N, T_w^*). Since k_r^* and h_s^* are involved together in the thermal resistance of the substrate [30], let $R_N = k_r^* h_s^*$ denote its variation. The function relationship of different characteristic angles with respect to R_N and T_w^* are investigated. Numerical computations of θ_1 and θ_2 are performed for 20 discrete points at $\{(R_N, T_w^*) : R_N = 0.125, 0.25, 0.387, 0.63, 0.75; T_w^* = 0, 0.5, 1, 1.5\}$, as shown in Fig. 9 (crosses). As previously, the response surfaces of θ_1 and θ_2 are constructed using the Kriging method; the results are displayed in Fig. 10. Then, the LOO cross validation is computed to assess the reliability of the constructed response surface. Here the maximum value of CV_s is 2.66% for $f_{\theta_1}(R_N, T_w^*)$ and 5.61% for $f_{\theta_2}(R_N, T_w^*)$, which implies that both surfaces are reliable enough, given that only 20 samples are used.

Furthermore, the forecast is also proceeded for six sample points, which are indicated by the circles in Fig. 9. The forecast results of θ_1 and θ_2 and the corresponding REs are shown in Table 3. Results reveal that for a water droplet evaporating on PTFE substrate with $T_w = 35\,°C$, i.e., $(R_N, T_w^*) = (0.48, 1.25)$, θ_1 and θ_2 are equal to 0.44 and 0.2172 in numerical work, while in the forecast approach, its value deviates from the RSM keeping 0.4272 and 0.2218 and the relative error is less than 3%. It is obvious that the forecast of θ_1 is as accurate as the previous (k_r^*, h_s^*) case. In addition, the forecast of θ_2 is less accurate (mean RE is 3.49%) than θ_1 due to a lower reliability of the response surface f_{θ_2}.

4.3.2. Coupling mechanisms on Marangoni flow

The Sobol sensitivity analysis is introduced to investigate the coupling mechanisms of Marangoni flow in two aspects: with or without heated substrate. The imposed temperature of a non-heated substrate equals to the ambient value $T_w = T_\infty$. While for a heated substrate T_w ranges from 20 °C to 50 °C. There is no doubt that the relationship between input and output variables shown in Figs. 8 and 10 is non-linear, which cannot be easily represented by a certain function. Therefore, we can use Sobol' index to analyse the sensitivity: higher Sobol' index implies higher sensitivity of the corresponding input parameter, and vice versa.

For droplet evaporating on a non-heated substrate, the Sobol index for k_r^* and h_s^* for the response surfaces plotted in Fig. 8 is computed: $S_{\theta_1}(k_r^*) = 81.31\%, S_{\theta_1}(h_s^*) = 15.95\%, S_{\theta_2}(k_r^*) = 68.39\%$, and $S_{\theta_2}(h_s^*) = 25.51\%$. It is obvious that the convective Marangoni flow reflected by θ_1 and θ_2 are much more sensitive with respect to k_r^* than h_s^*; this conclusion can also be observed in Fig. 8. The result also indicates that convective Marangoni flow strongly depends on the relative thermal conductivities: when the relative
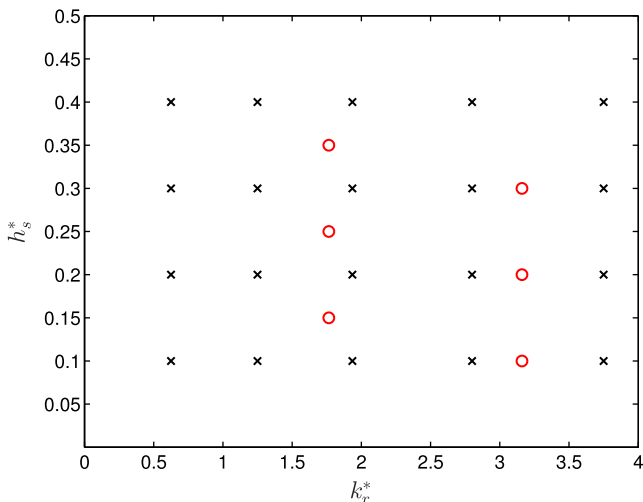

Fig. 7. Sample points for constructing response surface (crosses) and for forecasting the angles and the parameter estimation (circles).
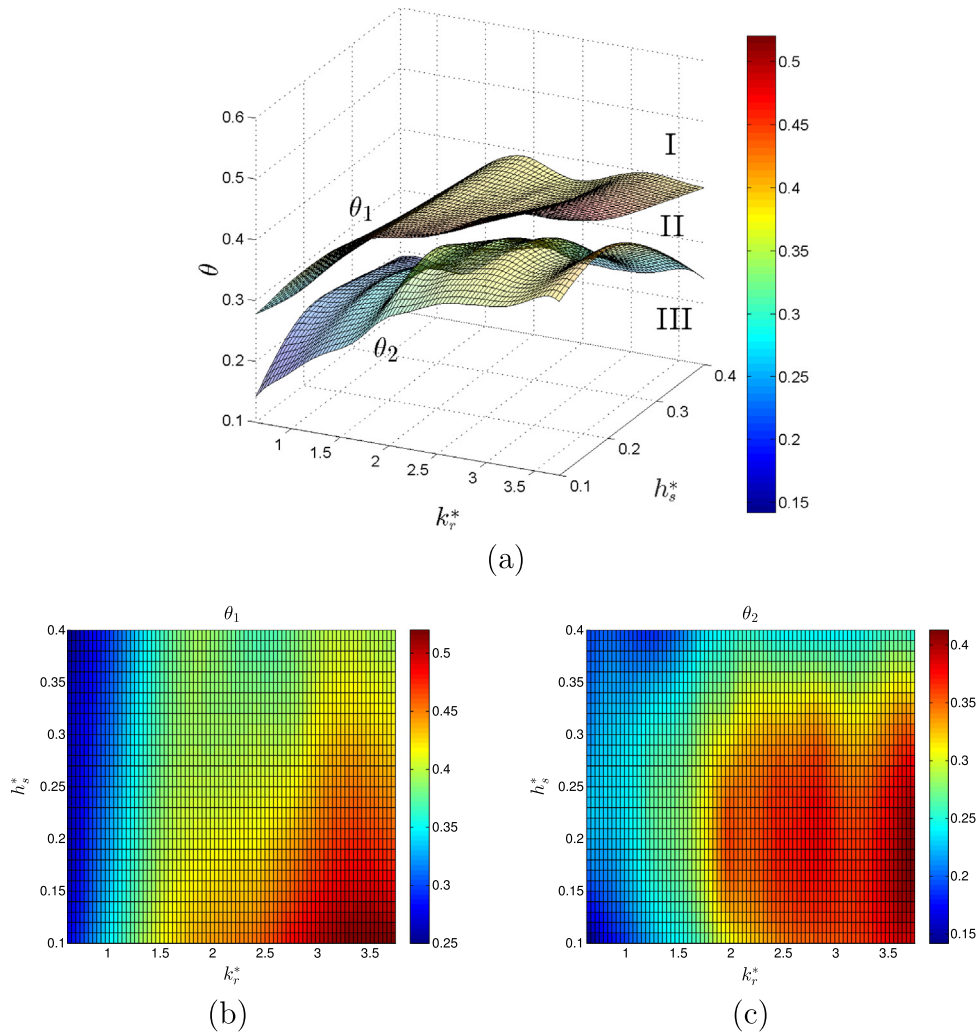
(a)

(b)

(c)

Fig. 8. (a) Response surface of θ_1 and θ_2 as a function of k_r^* and h_s^*, (b) projection of f_{θ_1}, (c) projection of f_{θ_2}.

Table 2
Forecast of θ_1 and θ_2 given k_r^* and h_s^* using the Kriging response surfaces.

(k_r^*, h_s^*)	Forecasting θ_1			Forecasting θ_2		
	Observation	RSM	RE (%)	Observation	RSM	RE (%)
(1.765, 0.15)	0.415	0.4145	0.13	0.34	0.3319	2.38
(1.765, 0.25)	0.383	0.3925	2.52	0.331	0.3208	3.07
(1.765, 0.35)	0.361	0.3818	5.76	0.236	0.2538	7.53
(3.16, 0.1)	0.502	0.5014	0.13	0.377	0.3648	3.23
(3.16, 0.2)	0.454	0.4529	0.19	0.384	0.3788	1.35
(3.16, 0.3)	0.416	0.4133	0.64	0.327	0.3472	6.17
Average			1.56			3.96

thermal conductivity changes a little, the convective multicellular flow changes a lot. On the other hand, the relative thickness has little impact on the resulting flow patterns due to its weak sensitivity.

In terms of heated substrates, Sobol' indices are also calculated: $S_{\theta_1}(R_N) = 99.06\%, S_{\theta_1}(T_w^*) = 1.15\%, S_{\theta_2}(R_N) = 42.9\%$, and $S_{\theta_2}(T_w^*) = 48.25\%$. It is remarkable that θ_1 is almost independent of T_w^*, so the substrate temperature has little influence on the appearance of the convective Marangoni flow. However, θ_2 is sensitive with respect to both influential parameters, indicating that thermal resistance of the substrate and substrate temperature have the same impact on the duration of the convective Marangoni flow.

4.3.3. Inverse problem

Typically, inverse problem relates to the situation that the input parameters cannot be accurately measured in some experiments. For example, the thickness of a very thin substrate is difficult to measure, since the contact measurement technique may destroy its surface structure. Thus, the thickness can be estimated by an indirectly method with the known numerical results containing the possible range and the Kriging-based response surface f_{θ_1} and f_{θ_2}. In what follows, we give an example to explain how to use the method to estimate the unknown parameters of k_r^* or h_s^*.

The inverse problem is considered for the six sample circles in Fig. 7. First, k_r^* is assumed to be an unknown parameter and is
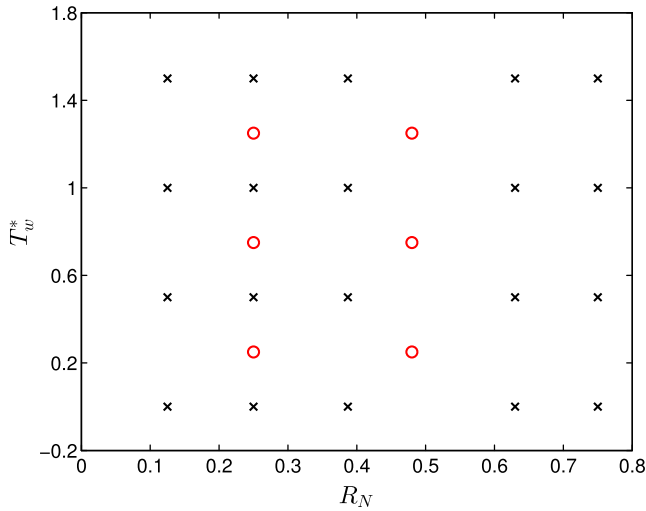
Fig. 9. Sample points for constructing response surface (crosses) and for forecasting the contact angles (circles).

error (RE) is also shown. It is observed that k_r^* is precisely estimated, except the two points (1.765, 0.25) and (1.765, 0.35), which are in a region less sensitive to k_r^* (see Fig. 8 (b)). Similarly to the forecast problem, the parameter estimation via the surface f_{θ_2} results in a higher error, as expected. Again, due to the lower reliability of the response surface and more local fluctuation, the estimation is less robust than using f_{θ_1}.

Similarly, in the case of unknown h_s^*, the parameter can also be estimated by the observed k_r^* and θ_i ($i = 1, 2$), as in the previous case. However, due to the low sensitivity of h_s^* with respect to θ_1 and θ_2, which is reflected by Sobol' indices (less than 11% for the both response surfaces), the estimation errors are relatively high, especially for the sample (1.765, 0.25) and (1.765, 0.35). The computation results are shown in Table 5. Furthermore, the estimates obtained from f_{θ_1} is more precise than f_{θ_2} due to the higher reliability of the constructed response surface.

We briefly conclude the use of the Kriging-based response surface and the strategy in the problem of forecasting the behaviour of Marangoni flow and the inverse problem. The observation of θ_2 is more irregular distributed than θ_1, such that the response surface is relatively less reliable. Therefore, in the forecast problem θ_1 can be more accurately given. For the same reason, it is well-advised to use the response surface f_{θ_1} in the parameter estimation problem. Besides, the estimation accuracy of input parameter in the inverse problem largely depends on the parameter sensitivity.
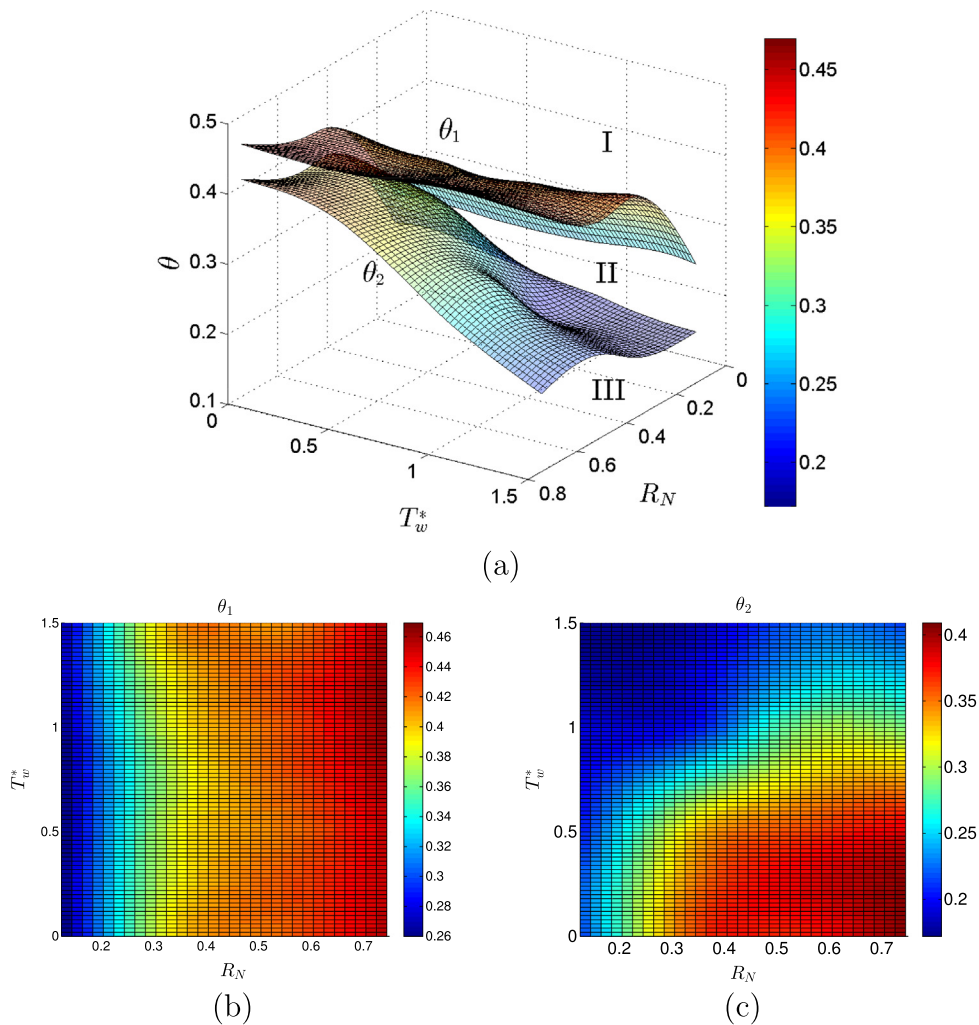
estimated by the measurements of h_s^* and θ_i^* ($i = 1, 2$) via Eq. (23). The estimation results are shown in Table 4. Here, $\hat{k}_r^*$ represents the estimation value of relative thermal conductivities, the relative

(a)

(b)

(c)

Fig. 10. (a) Response surface of θ_1 and θ_2 as a function of R_N and T_w^*, (b) projection of f_{θ_1}, (c) projection of f_{θ_2}.

Table 3
Forecast of θ_1 and θ_2 given R_N and T_w^* using the Kriging reponse surfaces.

(R_N, T_w^*)	Forecasting θ_1			Forecasting θ_2		
	Observation	RSM	RE (%)	Observation	RSM	RE (%)
(0.48, 0.25)	0.41	0.4369	4.12	0.364	0.392	7.69
(0.48, 0.75)	0.42	0.4209	0.22	0.302	0.3161	4.68
(0.48, 1.25)	0.44	0.4272	2.92	0.2172	0.2218	2.14
(0.25, 0.25)	0.351	0.3503	0.2	0.261	0.2646	1.39
(0.25, 0.75)	0.3605	0.3552	1.47	0.253	0.244	3.55
(0.25, 1.25)	0.36	0.3666	1.82	0.221	0.2176	1.53
Average			1.79			3.49

Table 4
Estimating k_r^* using the Kriging response surfaces θ_1 and θ_2.

(k_r^*, h_s^*)	Using θ_1		Using θ_2	
	$\hat{k}_r^*$	RE (%)	$\hat{k}_r^*$	RE (%)
(1.765, 0.15)	1.785	1.13	1.905	7.93
(1.765, 0.25)	1.585	10.2	2.465	39.66
(1.765, 0.35)	1.465	17	1.505	14.73
(3.16, 0.1)	3.185	0.79	3.345	5.85
(3.16, 0.2)	3.185	0.79	3.425	8.39
(3.16, 0.3)	3.305	4.59	2.665	15.66
Average		5.75		15.37

Table 5
Estimating h_s^* using the Kriging response surfaces θ_1 and θ_2.

(k_r^*, h_s^*)	Using θ_1		Using θ_2	
	$\hat{h}_s^*$	RE (%)	$\hat{h}_s^*$	RE (%)
(1.765, 0.15)	0.14	6.67	0.2	33.33
(1.765, 0.25)	0.32	28	0.2	20
(1.765, 0.35)	0.4	14.29	0.39	11.43
(3.16, 0.1)	0.1	0	0.15	50
(3.16, 0.2)	0.2	0	0.15	25
(3.16, 0.3)	0.29	3.33	0.29	3.3
Average		8.71		23.84

In this case, since both response surfaces are more sensitive to k_r^* than to h_s^*, the former can be well-estimated while the latter generally has a more imprecise estimate.

5. Conclusions

We have presented numerical computations on the evaporation of sessile droplets resting on a heated substrate. Special emphasis has been put on evaluating thermal effects of substrate on Marangoni flow in the course of evaporation. Three influential factors within thermal properties of substrate (e.g. relative thermal conductivity, relative substrate thickness and relative substrate temperature) have been investigated. We found a strong impact on the behaviours of Marangoni flow and clearly identified three characteristic bulk flow structures as a function of influential parameters when the contact angle diminishes with time during evaporation. These Marangoni flow patterns generated by the non-uniform temperature distribution along the interface allow to predict and control the evaporative deposition patterns. The underlying mechanism of the transition is primarily a result of matching the heat transfer from the substrate and heat flux losing through the liquid-gas interface, associated with evaporative cooling effect.

In order to better understand the Marangoni flow pattern with respect to the influential parameters in a wide range, a Kriging-based response surface method is proposed to forecast the flow patterns for any influential parameter in a given range. This approach, which only needs a limited number of simulations corresponding to a few discrete input parameters, has been applied successfully in the understanding of the hydrodynamics within evaporating droplets. The Sobol sensitivity analysis is recommended to quantify the relative importance of each influential parameter in determining the coupling mechanisms of Marangoni flow. The proposed method is also able to estimate the environmental parameters which may be ill-observed in the real situations. It is remarkable that the computational cost of Kriging-based response surface method and Sobol' sensitivity analysis is very low, particularly compared with the numerical simulation of Marangoni flow. Therefore, the combination of computer simulation and response surface method provides a useful guide to interpreting experimental results, especially in an uncertain environment.

Conflict of interest

None declared.

Acknowledgments

References

[1] M. Schena, D. Shalon, R. W Davis, P. O Brown, Quantitative monitoring of gene expression patterns with a complementary DNA microarray, Science 270 (5235) (1995) 467.

[2] Y.P. Chen, P. Cheng, Heat transfer and pressure drop in fractal tree-like microchannel nets, Int. J. Heat Mass Transfer 45 (13) (2002) 2643–2648.

[3] E. Forrest, E. Williamson, J. Buongiorno, L.W. Hu, M. Rubner, R. Cohen, Augmentation of nucleate boiling heat transfer and critical heat flux using nanoparticle thin-film coatings, Int. J. Heat Mass Transfer 53 (1) (2010) 58–67.

[4] K. Zhang, L.R. Ma, X.F. Xu, J.B. Luo, D. Guo, Temperature distribution along the surface of evaporating droplets, Phys. Rev. E 89 (3) (2014) 032404.

[5] S. Launay, V. Sartre, J. Bonjour, Parametric analysis of loop heat pipe operation: a literature review, Int. J. Therm. Sci. 46 (7) (2007) 621–636.

[6] R. Liu, Q.S. Liu, S.C. Zhao, Influence of rayleigh effect combined with marangoni effect on the onset of convection in a liquid layer overlying a porous layer, Int. J. Heat Mass Transfer 51 (25) (2008) 6328–6331.

[7] Z.Q. Zhu, Q.S. Liu, J.C. Xie, Experimental study on the combined evaporation effect and thermocapillary convection in a thin liquid layer, Microgravity Sci. Technol. 21 (1) (2009) 241–246.

[8] X. Chen, Z.Q. Zhu, Q.S. Liu, X.W. Wang, Thermodynamic behaviors of macroscopic liquid droplets evaporation from heated substrates, Microgravity Sci. Technol. 27 (5) (2015) 353–360.

[9] H. Hu, R. G Larson, Evaporation of a sessile droplet on a substrate, J. Phys. Chem. B 106 (6) (2002) 1334–1344.

[10] O.E. Ruiz, W.Z. Black, Evaporation of water droplets placed on a heated horizontal surface, J. Heat Transfer 124 (5) (2002) 854–863.

[11] F. Girard, M. Antoni, K. Sefiane, On the effect of Marangoni flow on evaporation rates of heated water drops, Langmuir 24 (17) (2008) 9207–9210.

[12] W.D. Ristenpart, P.G. Kim, C. Domingues, J. Wan, H.A. Stone, Influence of substrate conductivity on circulation reversal in evaporating drops, Phys. Rev. Lett. 99 (23) (2007) 234502.

[13] X.F. Xu, J.B. Luo, D. Guo, Criterion for reversal of thermal Marangoni flow in drying drops, Langmuir 26 (3) (2009) 1918–1922.

[14] C. Bouchenna, M.A. Saada, S. Chikh, L. Tadrist, Investigation of thermo-capillary flow inside an evaporating pinned water droplet, Interf. Phenomena Heat Transfer 3 (2) (2015).

[15] C. Bouchenna, M.A. Saada, S. Chikh, L. Tadrist, Generalized formulation for evaporation rate and flow pattern prediction inside an evaporating pinned sessile drop, Int. J. Heat Mass Transfer 109 (2017) 482–500.

[16] D.G. Krige, A statistical approach to some basic mine valuations problems on the Witwatersrand, J. Chem. Metall. Mining Soc. South Africa 52 (1951) 119–139.

[17] G. Matheron, Principles of geostatistics, Econ. Geol. 58 (1963) 1246–1266.

[18] B. Echard, N. Gayton, M. Lemaire, AK-MCS: an active learning reliability method combining Kriging and Monte Carlo Simulation, Struct. Safety 33 (2) (2011) 145–154.

[19] N. Gayton, J.M. Bourinet, M. Lemaire, CQ2RS: a new statistical approach to the response surface method for reliability analysis, Struct. Safety 25 (1) (2003) 99–121.

[20] J.C. Jouhaud, P. Sagaut, B. Labeyrie, A kriging approach for CFD/wind-tunnel data comparison, J. Fluids Eng. 128 (2006).

[21] T. Bracconier, M. Ferrier, J.C. Jouhaud, M. Montagnac, P. Sagaut, Towards an adaptive POD/SVD surrogate model for aeronautic design, Comput. Fluids 40 (2011) 195–209.

[22] X. Wang, S. Khazaie, L. Margheri, P. Sagaut, Shallow water sound source localization using the iterative beamforming method in an image framework, J. Sound Vib. 395 (2017) 354–370.

[23] S. Geisser, The predictive sample reuse method with applications, J. Am. Stat. Assoc. 70 (1975) 320–328.

[24] I. Sobol, Sensitivity estimates for non-linear mathematical models, Math. Model. Comput. Exp. 1 (4) (1993) 407–414.

[25] A. Saltelli, P. Annoni, I. Azzini, F. Campolongo, M. Ratto, S. Tarantola, Variance based sensitivity analysis of model output. design and estimator for the total sensitivity index, Comput. Phys. Commun. 181 (2) (2010) 259–270.

[26] X. Chen, P.G. Chen, J. Ouazzani, Q.S. Liu, Numerical simulation of sessile droplet evaporating on heated substrate, Eur. Phys. J. Special Top. 226 (6) (2017) 1325–1335.

[27] G.J. Dunn, S.K. Wilson, B.R. Duffy, S. David, K. Sefiane, The strong influence of substrate conductivity on droplet evaporation, J. Fluid Mech. 623 (2009) 329–351.

[28] R.D. Deegan, Pattern formation in drying drops, Phys. Rev. E 61 (1) (2000) 475.

[29] M.A. Saada, S. Chikh, L. Tadrist, Evaporation of a sessile drop with pinned or receding contact line on a substrate with different thermophysical properties, Int. J. Heat Mass Transfer 58 (1) (2013) 197–208.

[30] M.A. Saada, S. Chikh, L. Tadrist, Effect of substrate thickness and thermal conductivity on an evaporating sessile drop, Journal of Physics: Conference Series, vol. 395, IOP Publishing, 2012, p. 012140.